Supporting information for the article

Nuclear Spin Relaxation due to Chemical Shift Anisotropy of Gas-Phase ^{129}Xe

Matti Hanni, Perttu Lantto, and Juha Vaara

NMR Research Group
Department of Physics
P.O. Box 3000, FIN-90014
University of Oulu Finland

June 3, 2011

Contents

1 Redfield theory for CSA relaxation **1**

2 Molecular dynamics simulations **3**

3 Error sources **3**

4 Antisymmetric terms in CSA relaxation **4**

5 Figures and tables **5**

1 Redfield theory for CSA relaxation

The Redfield theory [1] is a weakly-coupled, semi-classical, statistical density matrix formulation for the time evolution of the nuclear magnetization $\mathbf{M} = n\gamma_K\hbar\langle\mathbf{I}_K\rangle$,[1] where n is the number density of nuclei, γ_K is the gyromagnetic ratio, and $\mathbf{I}_K$ is the dimensionless spin angular momentum operator of nucleus K. The NMR relaxation is caused by the fluctuations in the NMR tensors, parameters of the NMR spin Hamiltonian. The relaxation part of the time evolution of the component ε of $\mathbf{I}_K$ is, within the Redfield theory, governed by

$$\frac{d\langle I_\varepsilon\rangle}{dt} = \sum_{\alpha\alpha'\beta\beta'} R_{\alpha\alpha'\beta\beta'}\rho(t)_{\beta\beta'}(I_\varepsilon)_{\alpha'\alpha} = -\frac{\langle I_\varepsilon\rangle - \langle I_\varepsilon\rangle_0}{T} \tag{1a}$$

$$R_{\alpha\alpha'\beta\beta'} = J_{\alpha\beta\alpha'\beta'}(\omega_\alpha - \omega_\beta) + J_{\alpha\beta\alpha'\beta'}(\omega_{\alpha'} - \omega_{\beta'}) - \delta_{\alpha\beta}\sum_\sigma J_{\sigma\alpha'\sigma\beta'}(\omega_\sigma - \omega_{\beta'}) - \delta_{\alpha'\beta'}\sum_\sigma J_{\sigma\beta\sigma\alpha}(\omega_\sigma - \omega_\beta), \tag{1b}$$

where $R_{\alpha\alpha'\beta\beta'}$ is the Redfield matrix, α,β label the nuclear spin Zeeman states, and $\langle I_\varepsilon\rangle_0$ denotes a thermal equilibrium value. In Eq. (1a), a connection is made with the phenomenological Bloch equations, [2] enabling the identification of longitudinal ($T = T_1, \varepsilon = Z$) and transverse ($T = T_2, \varepsilon = X,Y; \langle I_\varepsilon\rangle_0 = 0$) relaxation times. $J(\omega)$ is the Fourier transform of the time autocorrelation function (TCF) $\langle H_{\alpha\beta}(0); H_{\beta'\alpha'}(t)\rangle$, of the perturbing, time-dependent NMR Hamiltonian $H(t)$:

$$J_{\alpha\beta\alpha'\beta'}(\omega) = \frac{1}{2}\int_{-\infty}^{\infty}\langle H_{\alpha\beta}(0); H_{\beta'\alpha'}(t)\rangle e^{-i\omega t}dt. \tag{2}$$

[1] We employ SI units throughout.

In the context of NMR relaxation processes, $H(t)$ is usually decomposed in terms of spherical tensor components

$$H(t) = \sum_{l=0}^{2} \sum_{q=-l}^{l} (-1)^q h_{(l,-q)}(t) A^{(l,q)}, \tag{3}$$

where $l = 0,1,2$ are the tensorial ranks of the time-dependent interaction tensor $h_{(l,-q)}(t)$ and time-independent spin operator $A^{(l,q)}$. In this approach, the SDF is written as

$$J_{\alpha\beta\alpha'\beta'}(\omega) = \sum_{l=0}^{2} \sum_{q=-l}^{l} j_{(l,-q)}(\omega) A^{(l,q)}_{\alpha\beta} A^{(l,q)*}_{\alpha'\beta'} \tag{4}$$

where the separation into spin-dependent and -independent terms is accomplished with the spectral density function (SDF) $j(\omega)$ written as

$$j_{(l,-q)}(\omega) = \int_0^\infty \langle h_{(l,-q)}(0); h_{(l,-q)}(t) \rangle \cos(\omega t) dt. \tag{5}$$

Hence, $j(\omega)$ is the Fourier transform of TCF consisting only of the time-dependent part of the perturbation Hamiltonian.

The interaction of nuclear spin with the static external magnetic flux density $\mathbf{B}_0$ can be written as

$$H^K_{\mathrm{NMR}} = -\frac{1}{2\pi} \gamma_K \mathbf{I}_K \cdot [\mathbf{1} - \sigma_K(t)] \cdot \mathbf{B}_0 \equiv h_{\mathrm{NZ}} + h_{\mathrm{CSA}}(t), \tag{6}$$

where σ_K is the nuclear shielding tensor. The unit tensor $\mathbf{1}$ accounts for the Zeeman interaction (NZ) of the bare nucleus. The Hamiltonian corresponding to shielding due to the electron cloud, $h_{\mathrm{CSA}}(t)$, is a small time-dependent perturbation. Its time-dependence arises from interatomic collisions, cluster formation, and the rotation of clusters with respect to $\mathbf{B}_0$. Due to the fact that $h_{\mathrm{CSA}}(t)$ appears twice in the SDF in Eq. (5), the CSA relaxation exhibits a built-in quadratic dependence on the external field.

The shielding tensor has a total of nine components, contributing to tensorial ranks 0, 1, and 2. The rank-0 part is a scalar corresponding to the shielding constant. It shifts the Zeeman levels by a constant amount, and thus is incapable of causing transitions between them. The rank-1 components cause the so-called antisymmetric (AS) effect on relaxation, which is often neglected, [3] although there are indications that it plays an important role in CSA relaxation in favorable conditions. [4, 5]

The most important, rank-2 part of the perturbation Hamiltonian (3) reduces to

$$H(t) = \sum_{q=-2}^{2} (-1)^q h^{\mathrm{CSA}}_{(-q)}(t) A^{(q)}, \tag{7}$$

where the label l = 2 is omitted for simplicity. The time-independent parts $A^{(q)}$ contain the external magnetic flux density. With the choice $\mathbf{B}_0 = (0,0,B_0)$ (external field along the Cartesian Z-axis of the laboratory frame), these are written as [6]

$$A^{(0)} = 2B_0 I_Z \quad ; \quad A^{(\pm 1)} = \mp \frac{\sqrt{6}}{2} B_0 I_\pm \quad ; \quad A^{(\pm 2)} = 0. \tag{8}$$

The necessary spherical components of the cylindrically symmetric and traceless reduced rank-2 shielding tensor are, consequently,

$$h_{(0)} = \frac{1}{2} \gamma_K \sigma_{ZZ} \quad ; \quad h_{(\pm 1)} = \frac{1}{\sqrt{6}} \gamma_K (\mp \sigma_{XZ} - i\sigma_{YZ}), \tag{9}$$

in terms of the Cartesian shielding tensor components $\sigma_{\varepsilon\kappa}$ $(\varepsilon, \kappa = X, Y, Z)$ with i the imaginary unit. The final perturbation Hamiltonian is thus

$$H(t) = B_0 \left[2h_{(0)} I_Z + \frac{\sqrt{6}}{2} h_{(-1)} I_+ - \frac{\sqrt{6}}{2} h_{(1)} I_- \right], \tag{10}$$

which implies a calculation of three distinct TCFs corresponding to the shielding tensor components $h_{(0)}$, $h_{(\pm1)}$. The overall TCF becomes (omitting constants)

$$\mathrm{TCF}(t) \propto \sum_{q=-1}^{1} \langle h_{(q)}(0); h_{(q)}(t)\rangle = \langle h_{(0)}(0); h_{(0)}(t)\rangle + 2\,\mathrm{Re}\langle h_{(1)}(0); h_{(1)}(t)\rangle - 2\,\mathrm{Im}\langle h_{(1)}(0); h_{(1)}(t)\rangle, \qquad (11)$$

since $\mathrm{Re}(h_1) = -\mathrm{Re}(h_{-1})$, and $\mathrm{Im}(h_1) = -\mathrm{Im}(h_{-1})$. The final shielding SDF used to calculate the CSA relaxation times T_1 is obtained by a Fourier transformation of Eq. (11), as

$$\mathscr{J}(\omega) = \mathscr{F}\{\mathrm{TCF}(t)\}, \qquad (12)$$

where $\mathscr{F}$ is used to denote Fourier transformation.

In the present work dealing with the CSA relaxation of monoatomic ^{129}Xe, the total shielding tensor for every Xe atom at each time step is constructed from the cylindrically symmetric tensors formed in the local dimer coordinate system. The dimer tensors are rotated to a common coordinate system, the laboratory frame, in which they are summed. Due to the cylindrical symmetry of the pair tensors, the small AS contributions to σ cannot be contained in the total PAA shielding tensor. Consequently, we assess the AS effect on the CSA T_1 by *a posteriori* -formulae (*vide infra*). [4]

2 Molecular dynamics simulations

The simulations were performed at the experimental number density and temperature points (n,T) [7, 8, 9, 10] with the GROMACS simulation package [11]. Velocity rescaling thermostat [12] and Berendsen [13] thermo-/barostat were used in NVT and NPT simulations, in which conditions were prepared for the production runs. The density was fixed by scaling the simulation box including 2000 atoms. The minimum image convention was used in connection with periodic boundary conditions. [14] After that, NVE production runs at the desired (n,T) points were carried out. The configurations were saved at each 1 fs time step of the 524.288 ps production runs, after an equilibration period of 300–500 ps. The total energy as well as temperature drifts were no greater than 0.3 kJ/mol and 2.2 K, respectively. The drifts remain within the rms error limits. A fully theoretical pair potential for Xe-Xe, obtained by combining coupled-cluster singles, doubles and perturbational triples [CCSD(T)] correlation treatment, scalar relativistic effects, bond basis functions, and core-polarization contributions, [15] was used in the simulations. The switching function [11] was used in the interatomic distance range of 1.95 – 2.15 nm, providing an *a priori* better choice than the simple truncation of potential due to the singularity in the force that follows from the latter. At the distance of 2.15 nm, the potential has a value of about 0.01% of its well depth. For comparison, we also employed the Aziz-Slaman potential, [16] and both a textbook Lennard-Jones (LJ) potential [17] and a LJ potential fitted to our own theoretical interaction potential. The fitting parameters ε = 2.354 kJ/mol and σ = 0.391 nm were obtained for the latter.

3 Error sources

The rms error of the height of the plateau in the example case of 295 K and 99.8 amg (See Figure 1 in the article) implies $\pm$5% error margins on T_1. The total TCF is governed by the h_{20} spherical shielding component, since the $h_{2\pm1}$ terms only contribute roughly 4% to the total T_1. Considering the statistical sampling over the xenon MD ensemble, the change in T_1 obtained between analyses of 200 and 2000 atoms (using only the h_{20} term) is comparable to the error in the Lorentzian fit.

Despite the fact that PAA was found to be successful for σ_{Xe} in Xe clusters, [18] the missing three-body and higher-order terms introduce an error to the analysis of CSA T_1. An estimate of the error due to PAA of the shielding tensors can be obtained from the coefficient of the linear regression fit of the PAA shielding anisotropies (constructed from the shielding anisotropy binary property surface) against quantum-chemically calculated shielding anisotropies (proportional to h_{20}) for the instantaneous clusters Xe_3–Xe_7 that occur in the present simulations. The differently coordinated atoms correspond to different slopes in this fit. Moreover, the number of differently coordinated atoms

is obtained from each simulated trajectory, which are used as weights of the slopes. Finally, a 5% error is obtained in the 295 K, 99.8 amg trajectory. This error is doubled in the TCF, implying $\pm$10% error margins for T_1 in this representative case. The binary shielding anisotropy curve is exact for the coordination number Z equal to unity, and the error in PAA increases for higher Z. [18] Hence, PAA involving the binary $\sigma_{\mathrm{Xe}}(r)$ becomes an increasingly good model at low densities.

The error estimate given for PAA is based on nonrelativistic Hartree-Fock calculations of the shielding tensors in the xenon clusters. This is due to the heavy computational burden that would arise from the calibration of quantum-chemical tensors for large clusters including the effects of electron correlation, relativity, and their coupling (see Eq. (10) of Ref. [19]). A total of ten HF calculations were performed for each cluster Xe_i, $i = 3 - 7$. In this context, the $\pm$10% error margins mentioned earlier should be considered as an order-of-magnitude estimate for the T_1.

4 Antisymmetric terms in CSA relaxation

The antisymmetric (AS) rank-1 parts of σ may contribute to CSA relaxation. [20] The AS parts are not included in our method, which essentially is a superposition of rank-2 $\sigma_{\mathrm{Xe}}(r)$ functions. Using approximate formulae for the T_1^{AS} (Eq. (5) in Ref. [4]), an *a posteriori* estimate of 10^{12} s is obtained, [21] with the minimum and maximum of ca. 10^6 s and 10^{14} s, respectively. The CSA T_1^{AS} is at least an order of magnitude larger than the rank-2 T_1 (Table 1 of the article). Thus, the AS components do not contribute significantly in the present case.

5 Figures and tables

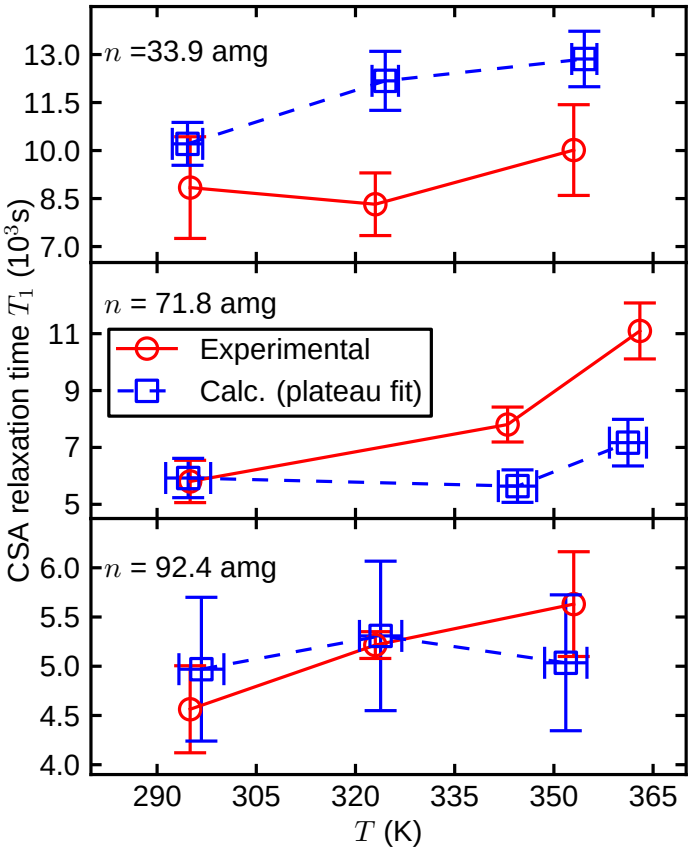

Figure 1: Temperature dependence of the calculated and experimental CSA relaxation times at three different number densities of 33.9, 71.8, and 92.4 amg.

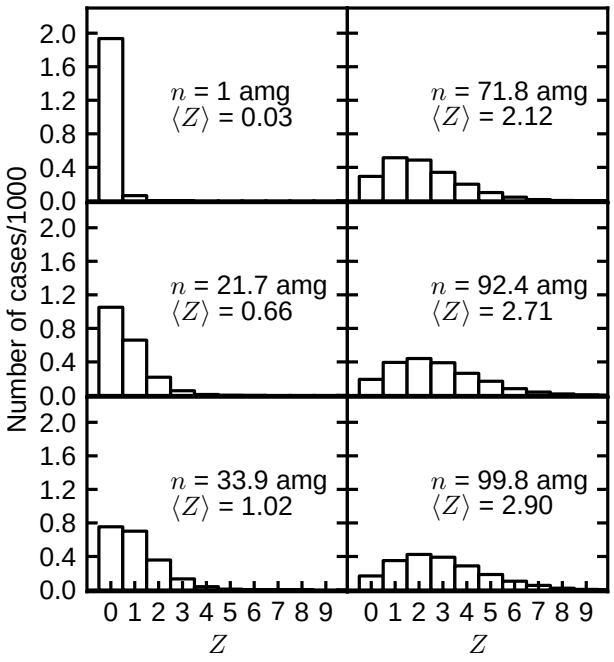

Figure 2: Density dependence of the calculated coordination number distribution in gaseous xenon at 295 K. In evaluating the coordination numbers we used the distance criterion of 6 Å corresponding to the first coordination shell of the highest-density Xe(*g*) simulation. The number-of-cases weighted average of the coordination number is obtained with $\langle Z \rangle = \frac{\sum_{Z=1}^{k} w_Z Z}{\sum_{Z=1}^{k} w_Z}$, where k and w_Z are the trajectory-specific highest occurring Z, and the number of atoms belonging to specific Z, respectively.

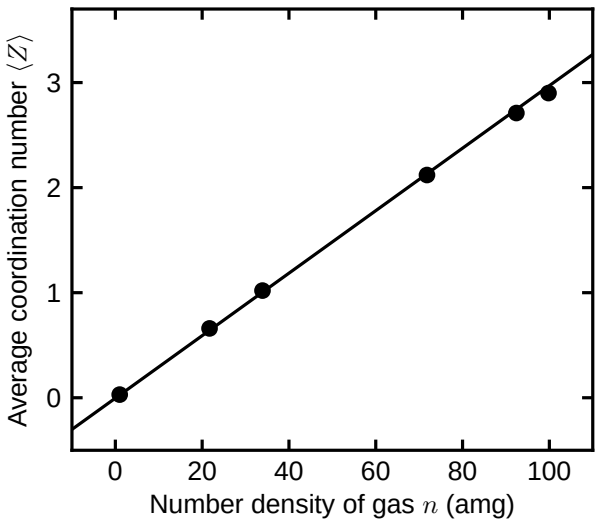

Figure 3: Simulated average coordination number $\langle Z \rangle$ of xenon atoms as a function of the number density in xenon gas at 295 K.

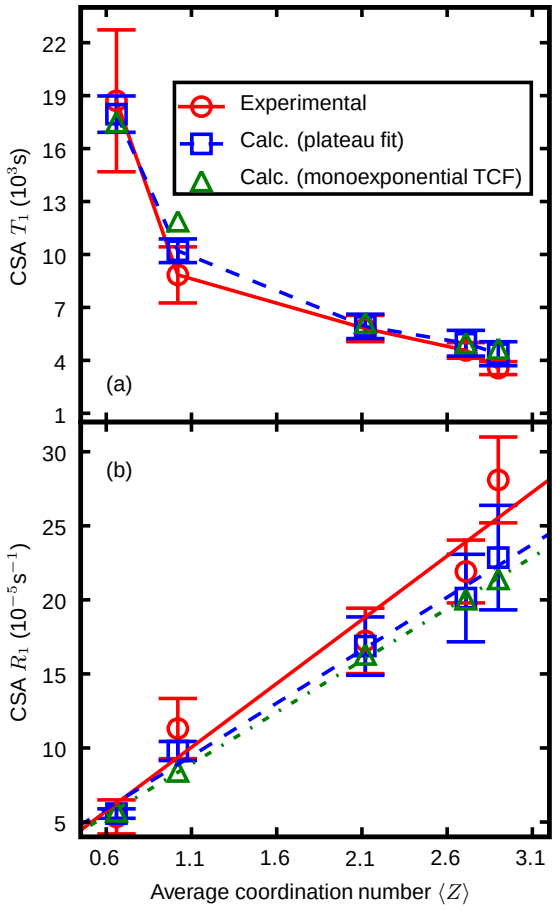

Figure 4: Calculated and experimental chemical shift anisotropy (a) relaxation times T_1 and (b) relaxation rates R_1, of xenon gas at 295 K as functions of the average coordination number.

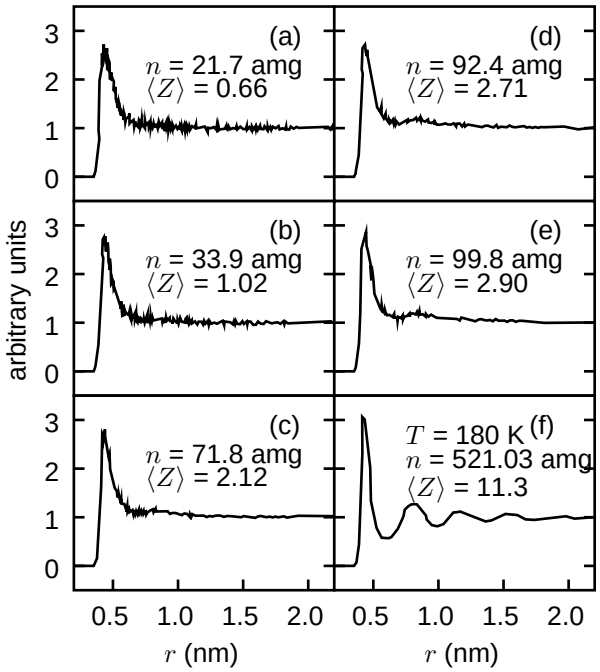

Figure 5: Calculated radial distribution functions (RDFs) of gaseous xenon (a-e) as functions of the number density at 295 K. The liquid phase RDF corresponding to 180 K and 521.03 amg is also shown in (f), along with the average coordination numbers.

Table 1: The parameters k, b and R^2 of the linear regression fit $y = kx + b$ for the experimental and the two theoretical (n, R_1) data sets in Figure 2 of the article.

method	k (10^{-6} s^{-1}/amg)	b (10^{-5} s^{-1})	R^2
expt.[a]	2.48	0.91	0.947
calc. plateau fit	2.06	1.89	0.989
calc. monoexp. TCF	2.01	1.53	0.999

[a] Ref. [7].

Table 2: Influence of the potential energy function and the physical content of the binary nuclear shielding tensor parametrization on the calculated ^{129}Xe chemical shift anisotropy relaxation time T_1 in gaseous xenon at 295 K and 99.8 amg.

Potential	Switch[a]	T_1 (s)[b]	Binary shielding[c]	T_1 (s)
Own[d]	on	4380	R, C, RCC[e]	4700[f]
	off	4040	R, C	4680
Own (0.5 fs MD step)	off	4120	R, NC	4630
LJ[g]	off	3010	NR, C	5870
Aziz-Slaman[h]	on	4220	NR, NC	5690

[a] Whether the switching function is used to eliminate the potential truncation artefacts, on = switching function used, off = no switching function.
[b] In all cases, the length of the shielding autocorrelation function is 524.288 ps with a time step of 1 fs, unless stated otherwise. All relaxation times presented here are calculated based on the Lorentzian fit of the plateau in the frequency domain, as explained in the footnote *c* of Table 1 in the article.
[c] R=relativistic, NR=nonrelativistic, C=correlated, NC=uncorrelated, RCC = including the coupling between relativity and correlation. Switch function used along with our best potential, Ref. [15]. Exactly the same microscopic positional data are used to calculate each of these T_1 values.
[d] Ref. [15]. Potential energy resulting from a counterpoise-corrected CCSD(T)/aug-cc-pVQZ/relativistic large-core effective core potential calculation featuring core polarization corrections as well as bond basis functions.
[e] R, C, RCC: full Eq. (10) of Ref. [19]; R, C: Breit-Pauli perturbation theory coupling between relativity and correlation omitted; R, NC: DHF shielding; NR, C: CCSD(T) shielding; NR, NC: HF shielding. These designations refer to the inclusion/omission of terms in Eq. (10) of Ref. [19].
[f] The seeming discrepancy between T_1 values of 4700 s and 4380 s (column 3 of the table) is due to the fact that they correspond to different microscopic positional data under the same experimental conditions. They reflect the error margins ($\pm$680 s at the conditions of this table) involved in the theoretical evaluation of T_1.
[g] The potential of Ref. [15] fitted to the Lennard-Jones functional form.
[h] The empirical Aziz-Slaman potential. [16]

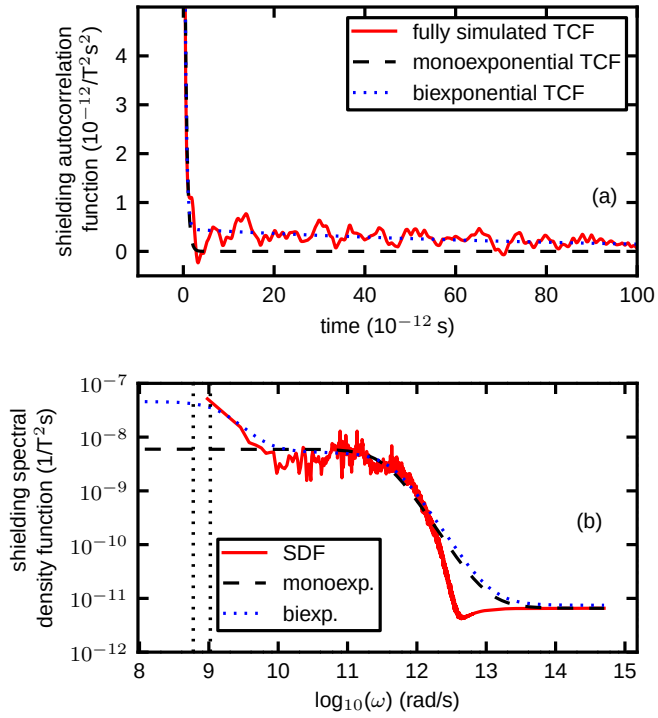

Figure 6: Simulated (a) shielding time autocorrelation function (TCF) (length of the analyzed, extended trajectory is 1048.576 ps), as well as the fitted mono- and biexponential decays and (b) the corresponding direct and two analytically Fourier-transformed spectral density functions (SDFs) of gaseous Xe at 1 amg and 295 K. The existence of two dimer species that correspond to different relaxation rates is suggested. In (b), the vertical dotted lines depict the ^{129}Xe Larmor frequencies $\omega_0 \approx 6.0\times10^8$ rad/s and 1.0×10^9 rad/s (B_0 of 8.0 T and 14.1 T, respectively).

References

[1] A. G. Redfield, *IBM J. Res. Develop.* **1957**, *1*, 19–31; *Adv. Magn. Reson.* **1965**, *1*, 1–32.

[2] F. Bloch, *Phys. Rev.* **1946**, *70*, 460–474.

[3] R. K. Harris, *Nuclear Magnetic Resonance Spectroscopy*, Longman, Harlow, **1986**.

[4] J. Kowalewski and L. Werbelow, *J. Magn. Reson.* **1997**, *128*, 144–148.

[5] R. Paquin, P. Pelupessy, L. Duma, C. Gervais, and G. Bodenhausen, *J. Chem. Phys.* **2010**, *133*, 034506.

[6] J. McConnell, *Phys. A* **1984**, *127*, 152–172.

[7] I. L. Moudrakovski, S. R. Breeze, B. Simard, C. I. Ratcliffe, J. A. Ripmeester, T. Seideman, J. S. Tse, and G. Santyr, *J. Chem. Phys.* **2001**, *114*, 2173–2181.

[8] M. V. Romalis and M. P. Ledbetter, *Phys. Rev. Lett.* **2001**, *87*, 067601.

[9] B. N. Berry-Pusey, B. C. Anger, G. Laicher, and B. Saam, *Phys. Rev. A* **2006**, *74*, 063408.

[10] B. C. Anger, G. Schrank, A. Schoeck, K. A. Butler, M. S. Solum, R. J. Pugmire, and B. Saam, *Phys. Rev. A* **2008**, *78*, 043406.

[11] B. Hess, C. Kutzner, D. van der Spoel, E. Lindahl, *J. Chem. Theory Comput.* **2008**, *4*, 435–447.

[12] G. Bussi, D. Donadio, and M. Parrinello, *J. Chem. Phys.* **2007**, *126*, 014101.

[13] H. J. C. Berendsen, J. P. M. Postma, W. F. van Gunsteren, A. DiNola, and J. R. Haak, *J. Chem. Phys.* **1984**, *81*, 3684–3690.

[14] M. P. Allen and D. J. Tildesley, *Computer Simulation of Liquids*, Clarendon Press, Oxford, **1987**

[15] M. Hanni, P. Lantto, N. Runeberg, J. Jokisaari, and J. Vaara, *J. Chem. Phys.* **2004**, *121*, 5908–5919.

[16] R. A. Aziz and M. J. Slaman, *Mol. Phys.* **1986**, *57*, 825–840.

[17] P. Atkins and J. de Paula, *Physical Chemistry*, Oxford University Press, **1996**. The Xe-Xe Lennard-Jones parameters used are ε = 1.779 kJ/mol and σ = 0.426 nm.

[18] M. Hanni, P. Lantto, and J. Vaara, *Phys. Chem. Chem. Phys.* **2009**, *11*, 2485–2496.

[19] M. Hanni, P. Lantto, M. Iliaš, H. J. Aa. Jensen, and J. Vaara, *J. Chem. Phys.* **2007**, *127*, 164313.

[20] J. Kowalewski and L. Mäler, *Nuclear Spin Relaxation in Liquids: Theory, Experiments, and Applications*, Taylor & Francis, **2006**.

[21] For the σ^{AS} components, we did Hartree-Fock calculations of 10 random Xe_{3-7} clusters, sampled from a 295 K, 99.8 amg trajectory. We use τ_2 = 1 ps.